OPEN ACCESS
IOP Publishing
Classical and Quantum Gravity
Class. Quantum Grav. **39** (2022) 065005 (25pp)
https://doi.org/10.1088/1361-6382/ac4fbb

Exactly solvable 2D model for photon propagation in curved space: loss of interference and Bell inequality violation

Karl-Peter Marzlin[1,*] **and Michael P Kinach**[1,2]

[1] Department of Physics, St. Francis Xavier University, Antigonish, Nova Scotia, B2G 2W5, Canada
[2] Department of Physics and Astronomy, University of British Columbia, 6224 Agricultural Road, Vancouver, British Columbia, V6T 1Z1, Canada

E-mail: pmarzlin@stfx.ca

Received 30 August 2021, revised 19 December 2021
Accepted for publication 13 January 2022
Published 28 February 2022

Abstract

We present an exact solution for the propagation of quantized massless scalar particles in a two-dimensional variation of the Alcubierre metric. Classical localized wavepacket solutions are derived using closed expressions for light-ray coordinates, and corresponding annihilation operators are constructed using the concept of locally positive and negative frequencies. The theory is used to describe the loss of fringe visibility in a single-photon interferometer, and the reduction of entanglement between two 2D photons, if one photon travels through a region with spacetime curvature. We derive an expansion of the field operator in terms of localized modes by means of an over-completeness relation. The quantization procedure also applies to massive and charged scalar fields in an n-dimensional globally hyperbolic spacetime.

Keywords: QFT, Alcubierre metric, photons, exact solutions

(Some figures may appear in colour only in the online journal)

1. Introduction

Exact solutions have always helped to sharpen our understanding of physical concepts. This is especially true for general relativity, where exact solutions to the Einstein equations are exceedingly rare. For quantum field theory in curved spacetime, most known solutions either

*Author to whom any correspondence should be addressed.

Original content from this work may be used under the terms of the Creative Commons Attribution 4.0 licence. Any further distribution of this work must maintain attribution to the author(s) and the title of the work, journal citation and DOI.

involve approximations or rely on a high degree of symmetry. In particular, the interpretation of fields as particles and anti-particles, or the identification of a vacuum state in curved space, is often considered to require a time-like Killing vector, so that energy conservation is ensured [1].

In this paper, we present an exactly solvable model for 2D photon propagation in a variation of the Alcubierre metric [2]. Our goal is to illustrate several aspects of wavepacket propagation in curved space. First, our metric has a high degree of flexibility, which provides us with a great level of control over the formation of horizons [3, 4]. Second, we provide an explicit example of how simultaneity, through the choice of a spacelike hypersurface, impacts the appearance of wavepackets.

Third, since our metric does not possess a timelike Killing vector, we quantize the field by introducing a set of localized creation and annihilation operators. This may be considered as a realization of local observables, which have been introduced within the framework of algebraic quantum field theory by Dimock [5] and further developed by several groups, including Hollands and Wald [6, 7], Sorkin [8], Afshordi *et al* [9], Brunetti *et al* [10], as well as Brunetti and Fredenhagen [11], Fredenhagen and Rejzner [12], and Bär and Ginoux [13, 14]. As an application of the general formalism, we demonstrate how spacetime curvature can affect quantum interference by reducing fringe visibility in a Mach–Zehnder interferometer, and how it reduces entanglement by testing the violation of the CHSH inequality [15] for a specific detector model.

Light propagation in an Alcubierre metric has been studied by Clark *et al* [16], Anderson *et al* [17] as well as Müller and Weiskopf [18] through ray tracing. Smolyaninov [19] has studied the simulation of classical light propagation in an Alcubierre metric using metamaterials. Hiscock [20] has studied the stress–energy tensor of a massless quantum field in a 2D Alcubierre metric.

Strictly speaking, our model does not deal with light, but with a massless scalar field in a two-dimensional spacetime. A 2D model cannot display all features that a quantized electromagnetic field in a 4D spacetime would exhibit. Since there are no transverse spatial degrees of freedom in a 2D spacetime, polarization of light and the dispersion of wavepackets will be absent. However, we nevertheless will refer to quantized wavepackets in our model as '2D photons' because many aspects of their dynamics and measurement closely resemble that of actual photonic wavepackets. Interference and entanglement of wavepackets are two aspects that we will study in detail.

The paper is organized as follows. In section 2, we will derive light-ray coordinates for a two-dimensional variation of the Alcubierre metric. These coordinates are used to examine light pulse propagation in section 3. In section 4, we will describe a quantization method that involves localized wavepackets of positive and negative frequencies to define mode operators for a general scalar field. This procedure is used in section 5 to study 2D photon propagation in our metric of interest. In section 6, we analyze a Mach–Zehnder interferometer and in section 7 we study violation of the CHSH inequality. Before we conclude, we derive an expansion of the field operator in terms of localized positive- and negative-frequency annihilation operators in section 8.

2. Light ray coordinates near a warp boundary

We consider a variation of the Alcubierre metric in two dimensions,

$$\mathrm{d}s^2 = -\mathrm{d}t^2 + (\mathrm{d}x - \dot{z}f(x-z)\mathrm{d}t)^2, \tag{1}$$

where $z(t)$ denotes the trajectory of the warp drive in the (t, x) coordinate system. Function $f(x)$ is a continuous function that goes to zero outside of the drive, and is close to unity inside the warp bubble. Generally, $f(x)$ is chosen to be nonzero only in a finite range, to represent a warp bubble of finite size. Here, we concentrate on the trailing edge of the bubble and consider a function that goes to zero for $x \to -\infty$ and to 1 for $x \to \infty$,

$$f(x) = \begin{cases} \frac{1}{2}\,\mathrm{e}^{2\sigma x} & x < 0 \\ 1 - \frac{1}{2}\,\mathrm{e}^{-2\sigma x} & x \geqslant 0. \end{cases} \tag{2}$$

The reason why we concentrate on one edge of the bubble is that the piecewise definition of $f(x)$ enables us to derive a closed expression for light-ray coordinates. The edge corresponds to the trailing end of the bubble for $\dot{z} > 0$, and to the leading edge for $\dot{z} < 0$. Our numerical examples will focus on the former case. $f(x)$ is differentiable, but its second-order derivative is discontinuous at $x = 0$, which results in a discontinuity of spacetime curvature.

For a given metric, light-ray coordinates $x_\pm$ can be derived by solving the equation for null geodesics,

$$\dot{x}^\mu \dot{x}^\nu g_{\mu\nu} = 0, \tag{3}$$

with $x^\mu = (t, x(t))$. In our case, a dot denotes a derivative with respect to t. For a given solution $x(t)$ of equation (3), light-ray coordinates can be derived by using the method of characteristics. This derivation is presented in appendix A. The result is

$$\bar{x}^{\mathrm{L}}_\eta(t, x) = -\frac{1}{2\sigma}\,\ln\left(\mathrm{e}^{-2\sigma(x+\eta t)} + L_\eta(t)\right) \tag{4}$$

$$\bar{x}^{\mathrm{R}}_\eta(t, x) = z(t_0) + \frac{1}{2\sigma}\,\ln\left(\mathrm{e}^{2\sigma(x+\eta t - z(t))} + R_\eta(t)\right), \tag{5}$$

with

$$L_\eta(t) = \sigma \int_{t_0}^{t} \mathrm{d}t' \dot{z}(t') \mathrm{e}^{-2\eta\sigma t' - 2\sigma z(t')} \tag{6}$$

$$R_\eta(t) = \sigma \int_{t_0}^{t} \mathrm{d}t' \dot{z}(t') \mathrm{e}^{2\eta\sigma t'}. \tag{7}$$

Superscripts L and R indicate that the solution is valid for the left region $x < z(t)$ or the right region $x > z(t)$, as displayed in figure 1. Parameter η specifies the general direction of motion of a light ray: $\eta = +1$ for left-moving light rays and $\eta = -1$ for right-moving rays. Hence, $\bar{x}^{\mathrm{L}}_+$ denotes light ray coordinates for left-moving rays in the region $x < z(t)$. Before the warp bubble starts to move, parameters L_η and R_η are zero. In this case, light ray coordinates are reduced to the expression in Minkowski space,

$$\bar{x}_\pm = x \pm t. \tag{8}$$

Unfortunately, light ray coordinates (4), (5) can only serve as a preliminary definition. The reason is that light rays generally cross the line $z(t)$, but coordinates $\bar{x}_\pm(t, x)$ are not continuous at $x = z(t)$. To fix this, we exploit that light ray coordinates are invariant under rescaling: any function $x_\eta(\bar{x}_\eta)$ of a light ray coordinate $\bar{x}_\eta$ can also be used as a light ray coordinate. The sketch in figure 1 shows our region of interest, i.e., a region of spacetime around trajectory

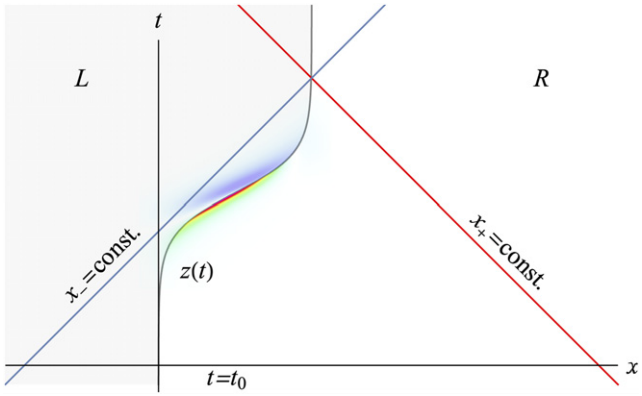

Figure 1. Sketch of light rays crossing the trajectory $z(t)$. The shaded region L corresponds to $x < z(t)$, and region R corresponds to $x > z(t)$. The colored area around $z(t)$ displays the Ricci scalar.

$z(t)$, which indicates the location of areas with large spacetime curvature. The colored area in figure 1 around the trajectory represents a contour plot of the Ricci scalar; details will be discussed below equation (19).

We assume that the warp drive is initially at rest. It is clear that, by moving the initial time t_0 sufficiently back into the past, we can ensure that all right-moving light rays that enter the region of interest will originate from the left area L. Furthermore, all left-moving rays will emanate from the right area, R. Before these rays cross the trajectory, the preliminary coordinates provide a suitable description for their dynamics. Hence, we set

$$x_-^{\mathrm{L}}(t,x) = \bar{x}_-^{\mathrm{L}}(t,x) \quad \text{for } x < z(t) \tag{9}$$

$$x_+^{\mathrm{R}}(t,x) = \bar{x}_+^{\mathrm{R}}(t,x) \quad \text{for } x > z(t). \tag{10}$$

To achieve continuity, we consider the preliminary coordinates $\tilde{x}_\eta(t) = \bar{x}_\eta(t, z(t))$ at point $x = z(t)$, where they are a function $\tilde{x}_\eta(t)$ of t alone,

$$\tilde{x}_\eta^{\mathrm{L}}(t) = -\frac{1}{2\sigma} \ln\left(\mathrm{e}^{-2\sigma(z(t)+\eta t)} + L_\eta(t)\right) \tag{11}$$

$$\tilde{x}_\eta^{\mathrm{R}}(t) = z(t_0) + \frac{1}{2\sigma} \ln\left(\mathrm{e}^{2\sigma\eta t} + R_\eta(t)\right). \tag{12}$$

For left-moving rays, we assume that, for $x < z(t)$, ray coordinates can be written in the form $\mathcal{F}(\bar{x}_+^{\mathrm{L}}(t,x))$. Continuity at $x = z(t)$ then imposes the condition $\mathcal{F}(\bar{x}_+^{\mathrm{L}}(t,z(t))) = x_+^{\mathrm{R}}(t,z(t))$, or equivalently, $\mathcal{F}(\tilde{x}_+^{\mathrm{L}}(t)) = \tilde{x}_+^{\mathrm{R}}(t)$. This implies that the function $\mathcal{F}$ is given by $\mathcal{F} = \tilde{x}_+^{\mathrm{R}} \circ \left(\tilde{x}_+^{L}\right)^{-1}$. In a similar way, we find $\mathcal{F} = \tilde{x}_-^{\mathrm{L}} \circ \left(\tilde{x}_-^{\mathrm{R}}\right)^{-1}$ for right-moving light rays. Hence,

$$x_-^{\mathrm{R}}(t,x) = \tilde{x}_-^{\mathrm{L}}\left(\left(\tilde{x}_-^{\mathrm{R}}\right)^{-1}\left(\bar{x}_-^{\mathrm{R}}(t,x)\right)\right) \quad \text{for } x > z(t) \tag{13}$$

$$x_+^{\mathrm{L}}(t,x) = \tilde{x}_+^{\mathrm{R}}\left(\left(\tilde{x}_+^{\mathrm{L}}\right)^{-1}\left(\bar{x}_+^{\mathrm{L}}(t,x)\right)\right) \quad \text{for } x < z(t). \tag{14}$$

This concludes the general derivation of light ray coordinates for a spacetime characterized by $f(x)$ of equation (2). Closed expressions for light ray coordinates can be provided if parameters $L_\eta(t)$ of equation (6) and $R_\eta(t)$ of equation (7) can be evaluated exactly. This is possible for special cases of the warp drive trajectory $z(t)$. For instance, for $z(t) = vt$, we obtain

$$L_\eta(t) = \frac{v}{2(\eta+v)}\left(\mathrm{e}^{-2\sigma t_0(\eta+v)} - \mathrm{e}^{-2\sigma t(\eta+v)}\right) \tag{15}$$

$$R_\eta(t) = \frac{v}{2\eta}\left(\mathrm{e}^{2\eta\sigma t} - \mathrm{e}^{2\eta\sigma t_0}\right). \tag{16}$$

In this case, if the warp drive is moving to the right at superluminal velocity v, right-moving light rays that are trailing the drive will fall behind, and 2D photons inside the warp drive will be dragged along with it. A warp drive moving at constant superluminal speed therefore forms a permanent horizon for light chasing the warp boundary.

For an accelerating warp drive, $z(t) = \frac{1}{2}at^2$, we find

$$L_\eta(t) = \frac{\sqrt{\pi\sigma}\eta\,\mathrm{e}^{\frac{\sigma}{a}}}{2\sqrt{a}}\left(\mathrm{erf}\left(\frac{at_0+\eta}{\sqrt{a/\sigma}}\right) - \mathrm{erf}\left(\frac{at+\eta}{\sqrt{a/\sigma}}\right)\right) + \frac{1}{2}\left(\mathrm{e}^{-\sigma t_0(at_0+2\eta)} - \mathrm{e}^{-\sigma t(at+2\eta)}\right) \tag{17}$$

$$R_\eta(t) = \frac{a}{4\sigma}\left(\mathrm{e}^{2\eta\sigma t_0} - \mathrm{e}^{2\eta\sigma t}\right) + \frac{a}{2\eta}\left(t\,\mathrm{e}^{2\eta\sigma t} - t_0\,\mathrm{e}^{2\eta\sigma t_0}\right). \tag{18}$$

In this case, 2D photons can still enter and leave the warp drive as long as its speed $\dot{z} = at$ is subluminal. A horizon is formed dynamically once the drive is sufficiently fast.

The focus of our study will be the case when a warp drive is only moving for a finite duration of time. A drive that could not perform such a type of motion would be of little practical use. In addition, from a theoretical perspective, a warp drive that only moves temporarily can dramatically simplify the physical interpretation. Before and after the warp drive moves, the Alcubierre metric will be flat. Far inside the warp drive, the metric is also flat, although t is not a time-like coordinate in that region anymore. Hence, a warp drive that moves for a finite period of time only produces curvature in a compact spacetime volume. It provides us with a controllable test case for analyzing the formation of temporary horizons and many other phenomena.

As a specific example, we consider the trajectory

$$z(t) = \frac{z_\mathrm{f}}{2}\left(1 + \tanh\left(\frac{2vt}{z_\mathrm{f}}\right)\right). \tag{19}$$

This describes a warp drive that starts at $z = 0$, accelerates to a maximum velocity v, and then decelerates until it reaches its final position z_f. Light ray coordinates then need to be evaluated numerically. The result is shown in figure 2. A 'temporary horizon' is opened up: right-moving light rays emanating from the left region in space can only catch up once the warp drive has slowed down. We note that figure 2 is a contour plot of light-ray coordinates $x_\pm(t, x)$, not the result of ray-tracing. From blue to orange, the value of x_+ in figure 2(a) varies from -7.82 to 10.12, and the value of x_- in figure 2(b) varies from -7.84 to 14.0. Possessing light-ray coordinates will enable us to introduce conformally Cartesian coordinates and to solve the wave equation below.

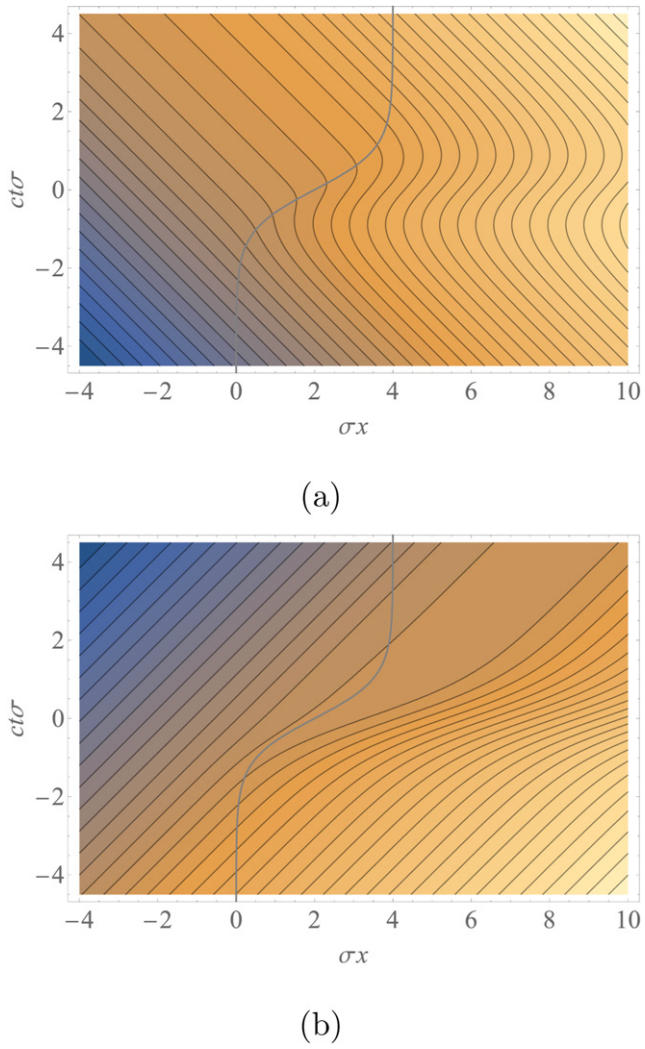

Figure 2. Contour plots of light ray coordinates for a warp drive that moves for a finite duration according to equation (19), with $z_\mathrm{f} = 4\sigma^{-1}$ and $v = 1.9$. (a) and (b) show left-moving coordinates $x_+(t, x)$ and right-moving coordinates $x_-(t, x)$, respectively. Trajectory $z(t)$ is shown as a gray line.

Trajectory (19) gives us very good control over the regions in spacetime with non-zero curvature. The colored area in figure 1 provides a contour plot of the Ricci scalar $\mathcal{R}$. Green and red correspond to positive values, and blue to negative values. In the right region R, the Ricci scalar is strictly positive and reaches a maximum of about $4v^2\sigma^2$. In the left region, $\mathcal{R}$ changes sign, with a maximum/minimum of about $\pm 3v^2\sigma/z_\mathrm{f}$. The last result is valid if the trip distance z_f is much larger than the width of the curvature area, $z_\mathrm{f}\sigma \gg 1$. In this limit, the curvature maximum in region R is significantly larger than in region L. As discussed before, the piecewise definition (2) of our metric leads to a discontinuity in curvature, but this effect has no significant consequences for our results.

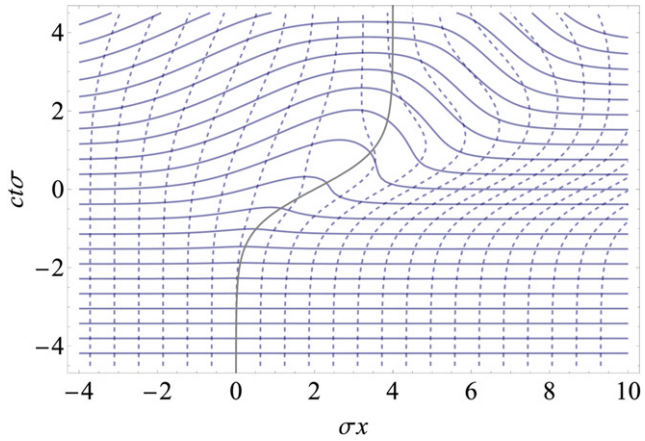

Figure 3. Lines of constant conformally Cartesian coordinates (T, X) for a warp drive that moves for a finite duration.

3. Pulse propagation

The main goal of this work is to study the propagation of light pulses and the description of 2D photons, i.e., quantized wavepackets. In this section, we first study the evolution of classical wavepackets. Since we consider a two-dimensional spacetime, we model light pulses by a massless scalar field $\psi(t, x)$ that obeys the wave equation in conformal coupling,

$$\nabla^\mu \nabla_\mu \psi(t, x) = 0. \tag{20}$$

Since the metric of a two-dimensional spacetime is conformally flat [21], it can be brought into the form

$$\mathrm{d}s^2 = (-\mathrm{d}T^2 + \mathrm{d}X^2) g_\Sigma(T, X), \tag{21}$$

where (T, X) are conformally Cartesian coordinates and g_Σ is the metric on a hypersurface of constant T. The wave equation then takes the explicit form $g_\Sigma^{-1}(\partial_X^2 - \partial_T^2)\psi = 0$. Conformally Cartesian coordinates are related to light ray coordinates via $x_\pm = X \pm T$. A plot of lines of constant X and T is given in figure 3.

The wave equation in light ray coordinates takes the form $\partial_{x_+}\partial_{x_-}\psi = 0$, which has the general solution

$$\psi(t, x) = \psi_+(x_+) + \psi_-(x_-). \tag{22}$$

It is not hard to show that light ray coordinates (4), (5) do indeed generate a solution of the wave equation for a metric specified by equations (1) and (2).

Having found the general solution, we need to specify the initial conditions for wavepackets. Our goal is to describe a wavepacket that, at conformal time $T = T_0$, takes a specific form $\psi_0(X)$ and travels in a specific direction. The first condition reads

$$\psi_0(X) = \psi(T_0, X) \;=\; \psi_+(X + T_0) + \psi_-(X - T_0). \tag{23}$$

To fix the initial direction of the pulse, we fix the 'time derivative' on the initial hypersurface. Specifically, let n^μ denote the time-like, future-oriented normal vector of the hypersurface. In conformally Cartesian coordinates, it takes the form $n^\mu = \sqrt{g_\Sigma}^{-1}(1, 0)$, so that

$\nabla_n = \sqrt{g_\Sigma}^{-1}\partial_T$. We now require that $\nabla_n\psi$ is equal to a given function $\psi_0^{(T)}(X)$ on the hypersurface,

$$\psi_0^{(T)}(X) = \nabla_n\psi(T,X)|_{T=T_0} \tag{24}$$

$$= \frac{1}{\sqrt{g_\Sigma}}\left(\frac{\partial x_+}{\partial T}\psi'_+(X+T_0) + \frac{\partial x_-}{\partial T}\psi'_-(X-T_0)\right) \tag{25}$$

$$= \frac{1}{\sqrt{g_\Sigma}}\left(\psi'_+(X+T_0) - \psi'_-(X-T_0)\right), \tag{26}$$

where a prime indicates a derivative with respect to the argument. Combining both initial conditions, we obtain

$$\psi_+(X+T_0) = \frac{1}{2}\left(\psi_0(X) + \int \mathrm{d}X\sqrt{g_\Sigma}\psi_0^{(T)}(X)\right) \tag{27}$$

$$\psi_-(X-T_0) = \frac{1}{2}\left(\psi_0(X) - \int \mathrm{d}X\sqrt{g_\Sigma}\psi_0^{(T)}(X)\right). \tag{28}$$

In order to obtain a wavepacket that is either left- or right-moving (depends either on x_+ or on x_- only), we have to choose the temporal derivative according to

$$\sqrt{g_\Sigma}\psi_0^{(T)}(X) = \eta\partial_X\psi_0(X), \tag{29}$$

with $\eta = \pm 1$.

We now analyze solutions of this type for a family of Gaussian wavepackets of the form

$$\Psi_{X_0,k}(T_0,X) = N\,\mathrm{e}^{\mathrm{i}k(X-X_0) - \frac{1}{2\Delta X^2}(X-X_0)^2}, \tag{30}$$

which are parameterized by the initial mean position X_0 and mean wavenumber k in conformally Cartesian coordinates. The width of the wavepackets is given by ΔX, and their peak height is equal to N. Since we know that the wavepacket only depends on one of the two coordinates x_+ or x_-, the corresponding solution is easy to find. Noting that $X = x_\eta - \eta T_0$, we obtain

$$\Psi_{X_0,k,\eta}(T,X) = N\,\mathrm{e}^{\mathrm{i}k(x_\eta - \eta T_0 - X_0) - \frac{1}{2\Delta X^2}(x_\eta - \eta T_0 - X_0)^2} \tag{31}$$

$$= N\,\mathrm{e}^{\mathrm{i}k(X - X_0 + \eta(T-T_0)) - \frac{1}{2\Delta X^2}(X - X_0 + \eta(T-T_0))^2}. \tag{32}$$

This simply corresponds to a Gaussian wavepacket that propagates to the left or to the right without changing its shape in conformally Cartesian coordinates.

Figure 4 shows a plot of three different Gaussian pulses in the (t,x) coordinate system instead of conformally Cartesian coordinates. All wavepackets have mean momentum $k = 0$. The only difference is their initial mean position X_0 and their initial direction; right-moving for figure 4(a), and left-moving for figure 4(b). The leftmost pulse starts in a region well outside of the warp drive. It is hardly disturbed by its motion and propagates like in a flat spacetime. This can be seen using equation (4): if $-\sigma(x \pm t) \gg 1$, the exponential factor in the logarithm dominates and we obtain $x_\pm \approx x \pm t$.

The rightmost pulse in figure 4 starts well within the warp drive, in a region that has very little spacetime curvature. The shape of this pulse is also undisturbed since it propagates through

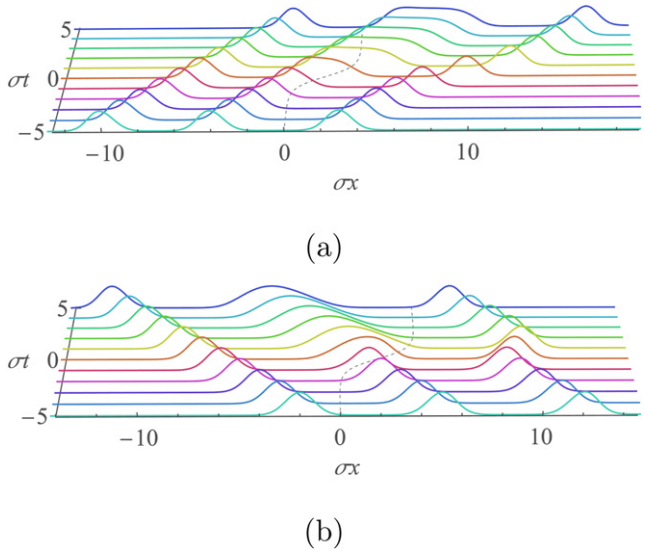

Figure 4. Propagation of Gaussian wavepackets. The leftmost packet starts well outside of the warp drive, the rightmost packet well within, and the center packet starts near the transition point $x = z(t)$. (a) and (b) show right-moving and left-moving wavepackets, respectively. The dashed line corresponds to trajectory $z(t)$.

a flat portion of spacetime. One can deduce this from equation (5): if $\sigma(x \pm t - z(t)) \gg 1$, the exponential factor in the logarithm dominates and we obtain

$$x_\pm \approx x \pm t - z(t). \tag{33}$$

The trajectory of a light ray that starts at $x_\pm = x_0$ is approximately given by $x = x_0 \mp t + z(t)$. Hence, the wavepacket is dragged along with the warp drive. We emphasize, however, that in this region t is not a time-like coordinate, so that the physical interpretation of the pulse is more subtle. We will come back to this when we discuss 2D photons below.

The center pulse in figure 4 passes through the region where the warp drive generates a large amount of curvature. Since curvature stretches the distance between light rays, it tears the pulse apart: parts of the pulse in the tail of the drive fall behind, while parts further inside are dragged along with the warp drive. As a result, the pulse gets stretched.

It is interesting to see the difference between the shape of the wavepacket on the two hypersurfaces of constant t and of constant T, respectively. In the (t, x) coordinate system, both hypersurfaces are straight horizontal lines before the warp drive is moving. Lines of constant T are deformed by the moving warp drive, and they remain curved even after the warp drive has stopped, see figure 3. The reason is that warp drive curvature generates a delay (or speed-up) in arrival times of light rays, and this delay persists. As a result, the wavepacket appears stretched and distorted on a hypersurface of constant t, as shown in figure 4. On the other hand, the wavepacket preserves its shape on the lines of constant T. This illustrates the well-known fact that the choice of a spacelike hypersurface can greatly influence the appearance of physical phenomena.

4. Pauli–Jordan quantization

To describe quantized wavepackets, we will employ a quantization method that postulates the commutation relations for the field operator $\hat{\phi}(x)$ through the Pauli–Jordan function (see, e.g., reference [1]),

$$[\hat{\phi}(x), \hat{\phi}^\dagger(y)] = \mathrm{i}G_{\mathrm{PJ}}(x,y). \tag{34}$$

In this section, we will keep the quantization method general and consider a Hermitian or charged, massive scalar field $\hat{\phi}(x)$ in an n-dimensional spacetime, which obeys the Klein–Gordon equation

$$\left(\nabla^\mu \nabla_\mu - m^2\right)\hat{\phi}(x) = 0, \tag{35}$$

where x denotes a set of n coordinates. The case of 2D photons can then be recovered by considering the Hermitian case and letting mass m go to zero. The Pauli–Jordan function is defined as the difference $G_{\mathrm{PJ}}(x,y) = G_{\mathrm{adv}}(x,y) - G_{\mathrm{ret}}(x,y)$ between advanced and retarded Green's function for equation (35). Lichnerowicz [22] has shown that both Green's functions exist in an open neighborhood of a point. They have support in the future and past light-cone, respectively, and are related through $G_{\mathrm{ret}}(x,y) = G_{\mathrm{adv}}(y,x)$. By construction, the Pauli–Jordan propagator is antisymmetric under exchange of x and y, and it is a solution to equation (35) with support inside and on the future and past light cone.

To introduce annihilation and creation operators for a specific mode, we employ the conserved scalar product on a spacelike hypersurface (see section 3.2 of reference [23])

$$\langle\psi|\phi\rangle = \mathrm{i}\int \mathrm{d}\Sigma\, \sqrt{g_\Sigma} n^\mu (\psi^* \partial_\mu \phi - (\partial_\mu \psi^*)\phi). \tag{36}$$

Here, n^μ is the normal vector ($n^\mu n_\mu = -1$) of the spacelike hypersurface that points into the future direction. g_Σ is the spatial metric on the hypersurface, such that $\mathrm{d}\Sigma\sqrt{g_\Sigma}$ gives the volume element, with $\mathrm{d}\Sigma = \mathrm{d}x_1 \wedge \mathrm{d}x_2 \wedge \cdots \wedge \mathrm{d}x_{n-1}$. This scalar product is preserved in the sense that it does not depend on the choice of the hypersurface if ψ, ϕ are solutions to the Klein–Gordon equation [24].

Scalar product (36) is not positive definite; a given solution ψ can have positive, negative, or zero value for $\langle\psi|\psi\rangle$. If it is positive, a wavepacket can be normalized according to $\langle\psi|\psi\rangle = 1$. Since the Klein–Gordon equation has real coefficients, a positive-norm solution ψ will induce a second solution ψ^* with negative norm $\langle\psi^*|\psi^*\rangle = -1$.

Mode operators can be defined through the scalar product of a wave packet $\psi(x)$ and the field operator [25],

$$\hat{a}_\psi(t) = \langle\psi|\hat{\phi}\rangle \tag{37}$$

$$\hat{b}^\dagger_{\psi^*}(t) = -\langle\psi^*|\hat{\phi}\rangle. \tag{38}$$

It is shown in appendix B that, for two positive-norm solutions $\psi(x), \chi(x)$ of the Klein–Gordon equation, the commutator between their annihilation operators is given by

$$[\hat{a}_\psi(\Sigma), \hat{a}^\dagger_\chi(\Sigma)] = \langle\psi|\chi\rangle. \tag{39}$$

Hence, for a state that is normalized to $\langle\psi|\psi\rangle = 1$, annihilation operator (37) obeys bosonic commutation relations.

In flat space, the interpretation of these operators is independent of an observer's reference frame: if a wavepacket is normalized to 1, then $\hat{a}_\psi$ can be interpreted as a bosonic annihilation operator for a positive-energy solution (a particle, for charged quantum fields) in mode $\psi(x)$, and $\hat{b}^\dagger_{\psi^*}$ as the creation operator for a corresponding negative-energy solution (an anti-particle). In curved space, the interpretation of these operators is generally ambiguous: what appears to be a particle (positive-energy solution) to one observer may appear to be an anti-particle (negative-energy solution) to another one. Related to this is the problem to define a global vacuum state: since the latter is defined by being annihilated by all operators $\hat{a}_\psi, \hat{b}_{\psi^*}$, a change in these operators implies a change in the vacuum state. However, this problem can be avoided in the context of algebraic quantum field theory [26]. There have also been proposals to introduce a local [27] or adiabatic vacuum state [28] to address the non-uniqueness of positive and negative energy solutions.

An unambiguous definition of a vacuum state is possible if spacetime possesses a time-like Killing vector. The associated symmetry implies conservation of energy, so that a global definition of positive and negative energies is possible. However, the Alcubierre metric does not possess a time-like Killing vector.

In this paper, we utilize the concept of locally positive and negative frequencies instead. More precisely, we consider the phase of the wavepacket by performing a Madelung transformation,

$$\psi = \sqrt{\rho}\, \mathrm{e}^{\mathrm{i}\alpha}. \tag{40}$$

Its norm then takes the form

$$\langle\psi|\psi\rangle = -2 \int \mathrm{d}\Sigma\, \sqrt{g_\Sigma}\, \rho\, n^\mu \nabla_\mu \alpha. \tag{41}$$

The sign of the norm is therefore directly related to the sign of the phase gradient $\nabla_n \alpha$: a phase gradient that is negative (positive) everywhere will lead to a positive (negative) norm, respectively. An example are energy eigenstates, for which $\alpha = -Et/\hbar$, so that $\partial_t \alpha = -E/\hbar$ is equal to the negative of the frequency $E/\hbar$ of the wave.

The condition $\nabla_n \alpha < 0$ everywhere is not necessary to ensure that $\langle\psi|\psi\rangle > 0$, but it is sufficient. Also, a wavepacket that fulfills $\nabla_n \alpha < 0$ everywhere on a spacelike hypersurface Σ_1 may evolve into a state for which the gradient is locally positive in some areas of another hypersurface Σ_2, but this would not affect its interpretation as a positive-frequency solution on Σ_1. In the following, we will show that it is possible to construct local positive-frequency wavepackets and to expand the field operator in terms of these states.

We remark that the condition $\nabla_n \alpha < 0$ can be linked to the initial value problem. Assume we know $\psi_0(x)$ and $\psi_0^{(T)}(x) = \nabla_n \psi(x)$ on the hypersurface. Using the Madelung transformation (40), we obtain the relation

$$\nabla_n \psi = \left(\frac{1}{2} \frac{\nabla_n \rho}{\rho} + \mathrm{i} \nabla_n \alpha \right) \psi. \tag{42}$$

Hence, by choosing $\psi_0^{(T)}$ in such a way that $\mathrm{Im}(\psi_0^{(T)}/\psi_0) < 0$, we can prepare a wavepacket that corresponds to a positive-frequency mode on the hypersurface.

5. 2D photons

In this section, we apply Pauli–Jordan quantization to obtain explicit expressions for 2D photon annihilation operators in a warp drive. We consider the creation of photons on a spacelike hypersurface characterized by constant conformal Cartesian time $T = T_0$. Their initial wavepacket $\psi_0(X)$ is of Gaussian shape (30). We consider left- or right-moving photons, and hence impose initial condition (29) as well. Normalization condition $\langle\psi|\psi\rangle = 1$ then becomes

$$1 = \mathrm{i}\eta \int_{-\infty}^{\infty} \mathrm{d}X \, (\psi_0^* \partial_X \psi_0 - \psi_0 \partial_X \psi_0^*) \tag{43}$$

$$= -2k\eta\sqrt{\pi}\Delta X |N|^2. \tag{44}$$

To find a positive-frequency solution, we must have $k\eta < 0$. For positive wavenumber k, the initial mean momentum would be positive, i.e., the wavepacket would be expected to move to the right. Right-moving wavepackets would correspond to the choice $\eta = -1$, and for this choice, the wavepacket can be normalized by setting $N = 1/\sqrt{-2k\eta\sqrt{\pi}\Delta X}$. Similarly, a positive norm is possible for negative k and $\eta = 1$. Other combinations, such as $k > 0, \eta = 1$, would describe negative-frequency solutions instead.

The time evolution of a photon can be derived in the same way as before and leads to result (32). In conformal Cartesian coordinates, a photon does not change its shape. Of particular interest is the analysis of the phase factor $\alpha = k(X - X_0 + \eta(T - T_0))$. In conformal Cartesian coordinates, its gradient is given by $\partial_T \alpha = k\eta$, which results in a positive mean frequency for $k\eta < 0$. In other words, the mean frequency does not change on hypersurfaces with constant T.

The situation is different if the wavepacket is considered on hypersurfaces with constant coordinate time t instead. Since $x_\eta = X + \eta T$, we then find the phase gradient

$$\partial_t \alpha = k \frac{\partial x_\eta}{\partial t}. \tag{45}$$

A plot of gradient (45) is shown in figure 5, in which shades of blue represent negative phase gradients, or positive frequency components. Dark blue corresponds to a frequency equal to, or larger than, the initial mean frequency. Light blue shades corresponds to positive frequencies that are lower in magnitude. Other colors represent negative frequencies.

One can see that an outside observer would interpret left-moving, positive-frequency waves localized inside the warp drive as negative-frequency waves. To understand this, we use approximation (33) for photons deep inside the warp drive, which yields $\partial_t \alpha \approx k(\eta - \dot{z})$. Assuming that $\dot{z} > 0$, this implies that the phase gradient changes its sign for left-moving waves ($\eta = 1$) for superluminal warp speed because they are dragged to the right by the warp drive. Photons co-moving with the warp drive ($\eta = -1$) always have the same sign of $\partial_t \alpha$, but their apparent frequency increases. However, since hypersurfaces of constant t are not spacelike inside the warp drive, this apparent change of frequencies is a coordinate effect with no physical consequences.

The situation is different for $t \gg \sigma^{-1}$, after the warp drive has come to rest. In this region, lines of constant coordinate time t are spacelike hypersurfaces. An observer who uses radar coordinates would likely use constant t to define simultaneity. In this coordinate system, photons that traveled through a region with curvature appear stretched as in figure 4, and their frequency is red-shifted, as shown by the light-blue areas in figure 5.

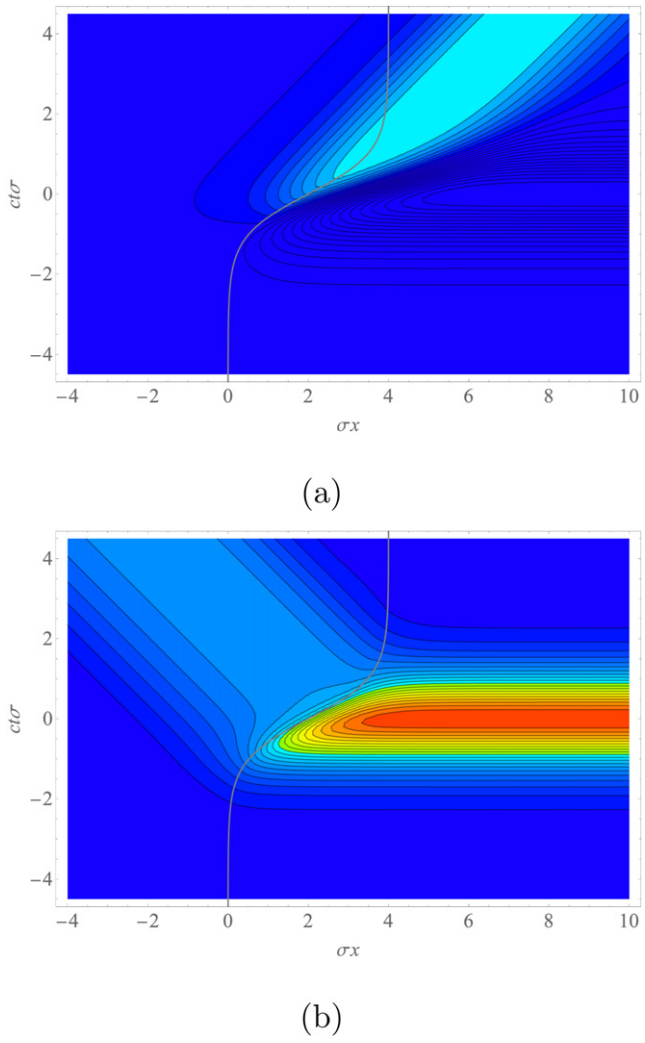

Figure 5. Contour plot of phase gradient (45) for (a) right-moving and (b) left-moving photons. Blue shades correspond to negative values, and other colors to positive values. Dark blue corresponds to a phase gradient of $-|k|$ or lower. Red to $|k|$ or higher.

On the other hand, an observer who moves along with the warp drive would likely consider a line of constant conformal time T (see figure 3) as a spacelike hypersurface. In this coordinate system, photons would appear undistorted and with unchanged frequency. This provides an explicit example of how, even in a flat region of spacetime, two observers may disagree on the interpretation of a wavepacket. The choice of a hypersurface can therefore have direct consequences for the quantum measurement process, which involves an instantaneous projection of the quantum state. We conjecture that the measurement process should be described using the rest frame of the detection device to define instantaneity, and we will use this assumption in sections 6 and 7. The example provided here also supports the idea that the concept of a particle is linked to simultaneity [29].

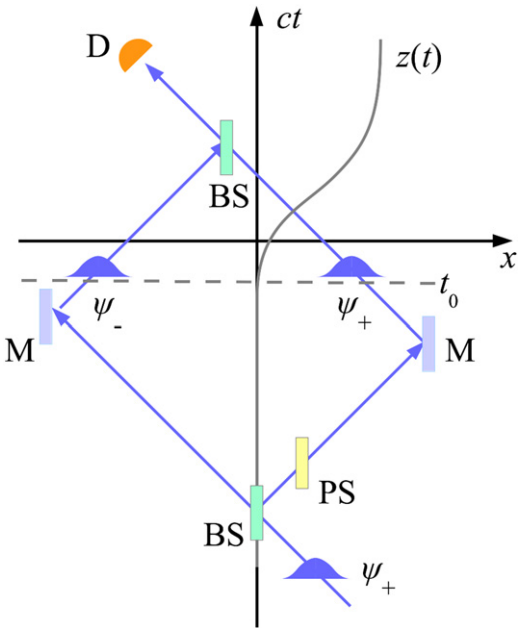

Figure 6. Mach–Zehnder interferometer in an Alcubierre metric. A single left-moving wavepacket ψ_+ passes through a beam splitter BS, a phase shifter PS, and two mirrors M to create a superposition of two single-photon wavepackets at time t_0. The resulting interference pattern is measured by a detector D after the warp drive comes to rest.

6. Mach–Zehnder interferometer

As a first application of the quantization scheme presented above, we study the interference of a single 2D photon pulse in the Mach–Zehnder interferometer shown in figure 6. A 2D photon is prepared in wavepacket ψ_+ and then hits a beam splitter BS, which creates a 50–50 superposition of the original wavepacket ψ_+ and a reflected wavepacket ψ_-. The reflected wavepacket passes through a phase shifter PS, which multiplies the wavefunction with an adjustable phase factor $\mathrm{e}^{\mathrm{i}\theta}$. This is needed to observe an interference pattern. The two wavepackets are reflected by two mirrors M. A perfect mirror at position x_B can be modeled as a boundary condition $\psi(x_\mathrm{B}, t) = 0$. In flat space, this boundary condition can be fulfilled by the method of mirror images. An incoming wavepacket $\psi_-(x - t)$ would then reflected as $-\psi_-(2x_\mathrm{B} - x - t)$, which we denote as left-moving wave ψ_+ in the figure.

In our thought experiment, all the steps described so far happen at a time t_0 before the warp drive starts to move, i.e., in flat space. Their combined effect is to create the quantum state

$$|\psi(t_0)\rangle = \frac{1}{\sqrt{2}}\left(\hat{a}_-^\dagger + \mathrm{e}^{\mathrm{i}\theta}\hat{a}_+^\dagger\right)|0\rangle. \tag{46}$$

Wavepacket ψ_+ then propagates through the region with spacetime curvature. After the warp drive stopped, a second beam splitter recombines the two wavepackets, and the left output signal is registered by a detector D. A perfect beam splitter at position x_BS lets a photon pass with a 50% chance, or it reflects the photon like a perfect mirror. We denote a reflected wavepacket with a subscript R. The quantum state after the second beam splitter is given by (see section 8.3

of reference [30])

$$|\psi(t_{\rm f})\rangle = \frac{1}{2}\left(e^{i\theta}\hat{a}^\dagger_+ + \hat{a}^\dagger_{-,\rm R}\right)|0\rangle + \frac{1}{2}\left(\hat{a}^\dagger_- - e^{i\theta}\hat{a}^\dagger_{+,\rm R}\right)|0\rangle. \tag{47}$$

The first part on the right-hand side corresponds to the wavepacket that leaves the final beam splitter to the left and arrives at the detector.

We model beam splitter and detector as material objects that move on a time-like geodesic, which we take as lines of constant x in the (t, x) coordinate system. Consequently, the direction of time in the rest frame of the beam splitter is ∂_t, so that, in this coordinate system, reflection can be defined in exactly the same way as in flat space. Furthermore, by monitoring the left output port of the beam splitter, we only have to consider the reflection of wavepacket ψ_-, which always travels through flat space.

An ideal single-photon detector is a projector on the single-particle subspace of Fock space. Since a detector only has a finite size, it can only detect photons that hit the detector surface. One can therefore think of the detector as projection on a detector mode $\psi_{\rm D}(x)$. The detector's projector then takes the form $\hat{P}_{\rm D} = \hat{a}^\dagger_{\rm D}|0\rangle\langle 0|\hat{a}_{\rm D}$. The process of projection needs to be modeled on a specific spacelike hypersurface, which under our assumptions is also characterized through normal vector $n = \partial_t$. The detection signal is then given by

$$S = \langle\psi(t_{\rm f})|\hat{P}_{\rm D}|\psi(t_{\rm f})\rangle \tag{48}$$

$$= \frac{1}{4}\left|e^{i\theta}\langle\psi_{\rm D}|\psi_+\rangle + \langle\psi_{\rm D}|\psi_{-,\rm R}\rangle\right|^2. \tag{49}$$

Signal S can be affected through gravity via two effects. One is simply the displacement of wavepacket ψ_+ as it is dragged along with the warp drive. If the two wavepackets are not both inside the detector at detection time, S will trivially be zero. We therefore assume that the left mirror in figure 6 will always be adjusted in such a way that both wavepackets arrive simultaneously at the detector. Under this assumption, factor $\langle\psi_{\rm D}|\psi_{-,\rm R}\rangle$ will be the same for all interferometric setups. For simplicity, we assume that the detector is optimized to measure mode $\psi_{-,\rm R}$, so that $\langle\psi_{\rm D}|\psi_{-,\rm R}\rangle = 1$. The interference signal then takes the form

$$S = \frac{1}{4}\left(1 + |\langle\psi_{\rm D}|\psi_+\rangle|^2 + 2|\langle\psi_{\rm D}|\psi_+\rangle|\cos(\theta + \Delta\theta)\right), \tag{50}$$

where $\Delta\theta = \arg(\langle\psi_{\rm D}|\psi_+\rangle)$ is a curvature-induced phase shift. By varying the phase θ of the phase shifter, we can observe the interference between the two single-photon wavepackets.

For an interferometer, fringe visibility is conventionally defined as

$$V = \frac{S_{\max} - S_{\min}}{S_{\max} + S_{\min}} \tag{51}$$

$$= \frac{2|\langle\psi_{\rm D}|\psi_+\rangle|}{1 + |\langle\psi_{\rm D}|\psi_+\rangle|^2}. \tag{52}$$

It is not hard to see that the signal then takes the form $S \propto 1 + V\cos(\theta + \Delta\theta)$. We have numerically evaluated phase shift $\Delta\theta$ and fringe visibility V for wavepackets that at time $t_0 = -5.0\sigma^{-1}$ have the form (30), with $k = 100\sigma$ and $\Delta X = 0.3\sigma^{-1}$, and which are detected at time $t = 5.0\sigma^{-1}$. The result is shown in figure 7. When wavepacket ψ_+ starts sufficiently far to the left, it only travels through flat space. As a consequence, the overlap with the detector is perfect and no phase shift is induced. For larger values of the wavepacket's initial position x_0, it will travel through the region of curvature induced by the warp drive. This will

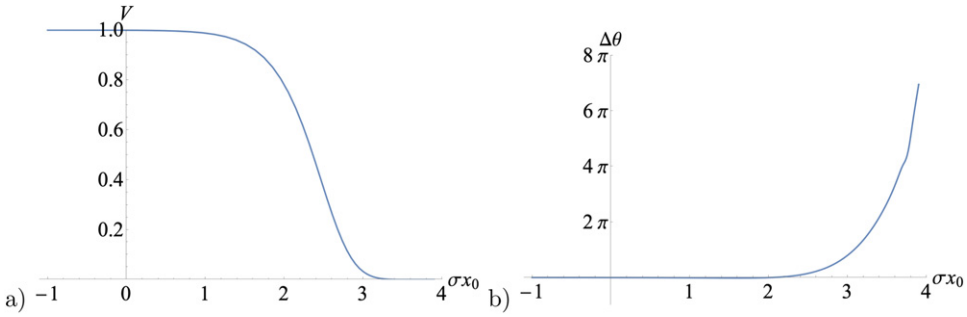

Figure 7. Fringe visibility (a) and phase shift (b) for an interferometer that is affected by a warp drive.

modify the wavepacket to such an extent that fringe visibility is reduced to near zero. We have verified through a numerical Fourier transformation that the dominant cause for the loss of fringe visibility is the change in the photon's mean momentum $\hbar k$, rather than the deformation of the wavepacket envelope. The reason is that for our choice of parameters the mean wavelength $2\pi/k$ is much smaller than the width ΔX of the wavepacket. Consequently, its width in momentum space is narrow and a gravitationally induced change in mean momentum will quickly reduce the overlap with the detector mode in momentum space. Curvature also induces a phase shift $\Delta\theta$, but the phase shift is only large for very small fringe visibility.

7. Violation of the Bell inequality

One of the most fundamental tests of quantum physics is the violation of the Bell inequality [31], or the experimentally more convenient CHSH inequality [15],

$$|\langle AB + A'B + AB' - A'B'\rangle| \leqslant 2, \tag{53}$$

with four dichotomic random observables A, A', B, B' that each can only take values ± 1. It is fulfilled for classical random variables provided that measuring observables A, A' is not influenced in any way by measuring B, B' and vice versa. In quantum physics, the observables are described by operators $\hat{A}, \hat{A}', \hat{B}, \hat{B}'$ with eigenvalues ± 1, for which the CHSH inequality can be violated [32]. A common choice of observables are related to spin-$\frac{1}{2}$ particles. If $\hat{\vec{\sigma}}$ denotes the vector of Pauli matrices, the four observables take the form $\hat{A} = \vec{n} \cdot \hat{\vec{\sigma}}$ with unit vector $\vec{n} = (\cos\,\phi_a\,\sin\,\theta_a, \sin\,\phi_a\,\sin\,\theta_a, \cos\,\theta_a)$ and similarly for the other three observables with angles $\theta_{a'}, \theta_b, \theta_{b'}, \phi_{a'}, \phi_b, \phi_{b'}$. For the choice $\phi_i = 0, i = a, a', b, b'$ as well as $\theta_a = 0$, $\theta_{a'} = \frac{\pi}{2}$ and $\theta_b = \frac{\pi}{4} = -\theta_{b'}$, the Bell operator takes the specific form

$$\hat{\mathcal{B}} = \hat{A} \otimes \hat{B} + \hat{A}' \otimes \hat{B} + \hat{A} \otimes \hat{B}' - \hat{A}' \otimes \hat{B}' \tag{54}$$

$$= \sqrt{2}\,(\hat{\sigma}_x \otimes \hat{\sigma}_x + \hat{\sigma}_z \otimes \hat{\sigma}_z)\,. \tag{55}$$

For the entangled state $|\psi\rangle = \frac{1}{\sqrt{2}}(|\uparrow\downarrow\rangle - |\downarrow\uparrow\rangle)$ its mean value is given by $\langle\psi|\hat{\mathcal{B}}|\psi\rangle = -2\sqrt{2}$, which corresponds to a maximal [33] violation of the CHSH inequality.

Bell inequality violation (BIV) can be obtained for many different systems. A simple way to achieve this is to replace the Pauli matrices by three other operators $\hat{\sigma}_i$ that obey the same

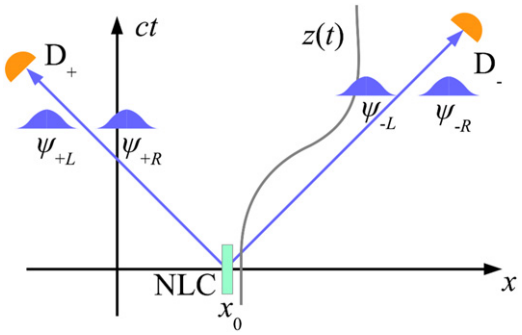

Figure 8. Test of the CHSH inequality in an Alcubierre metric. A nonlinear crystal NLC creates a pair of 2D photons that travel in opposite directions and are each in a superposition of two displaced wavepackets L and R. The CHSH inequality is tested using two separate detectors $D_\pm$.

commutation relations. For continuous variables like position and momentum, these operators may include parity and two other variables that test even and odd wavefunctions [34–38]. In this paper, we will exploit the Jordan–Schwinger representation of Lie algebra su(2) to analyze the thought experiment sketched in figure 8. A nonlinear crystal NLC generates pairs of entangled 2D photons that leave the crystal in opposite directions. To generate entanglement, we use time-bin encoding, for which BIV has been experimentally demonstrated by Marcikic *et al* [39]. In time-bin encoding, a qubit is encoded into two identical wavepackets, which at a given time t are spatially displaced relative to each other. The left-moving '+' photon starts in a superposition of $\psi_{+\mathrm{L}}(x)$ and $\psi_{+\mathrm{R}}(x)$, corresponding to two wavepackets that are displaced to the left (L) and to the right (R), respectively. For perfect encoding, the overlap between the two wavepackets would vanish, $\langle\psi_{+\mathrm{R}}|\psi_{+\mathrm{L}}\rangle = 0$. Similarly, the right-moving photon is in a superposition of $\psi_{-\mathrm{L}}(x)$ and $\psi_{-\mathrm{R}}(x)$. We consider the situation that initially all four wavepackets have vanishing overlap and that the left-moving photon will always travel through a flat portion of spacetime, so that it will not change its shape.

To analyze BIV in the presence of gravity, the two photons are prepared in the entangled state

$$|\psi\rangle = \frac{1}{\sqrt{2}}\left(\hat{a}^\dagger_{+\mathrm{R}}\hat{a}^\dagger_{-\mathrm{R}} + \hat{a}^\dagger_{+\mathrm{L}}\hat{a}^\dagger_{-\mathrm{L}}\right)|0\rangle. \tag{56}$$

This is done before the warp drive starts moving, so that all creation operators take the same form as in flat space. The two detectors $D_\pm$ in figure 8 measure Bell observables that are defined through the Jordan–Schwinger representation of su(2),

$$\hat{\sigma}_{x\pm} = \hat{a}^\dagger_{\bar{\psi}_{\pm\mathrm{L}}}\hat{a}_{\bar{\psi}_{\pm\mathrm{R}}} + \hat{a}^\dagger_{\bar{\psi}_{\pm\mathrm{R}}}\hat{a}_{\bar{\psi}_{\pm\mathrm{L}}} \tag{57}$$

$$\hat{\sigma}_{y\pm} = \mathrm{i}\hat{a}^\dagger_{\bar{\psi}_{\pm\mathrm{L}}}\hat{a}_{\bar{\psi}_{\pm\mathrm{R}}} - \mathrm{i}\hat{a}^\dagger_{\bar{\psi}_{\pm\mathrm{R}}}\hat{a}_{\bar{\psi}_{\pm\mathrm{L}}} \tag{58}$$

$$\hat{\sigma}_{z\pm} = \hat{a}^\dagger_{\bar{\psi}_{\pm\mathrm{R}}}\hat{a}_{\bar{\psi}_{\pm\mathrm{R}}} - \hat{a}^\dagger_{\bar{\psi}_{\pm\mathrm{L}}}\hat{a}_{\bar{\psi}_{\pm\mathrm{L}}}. \tag{59}$$

Here, $\bar{\psi}_{\pm\mathrm{R}}$ and $\bar{\psi}_{\pm\mathrm{L}}$ are the wavepackets to which the detectors are sensitive at the time of measurement. Since the detection happens after the warp drive stopped, we can again define

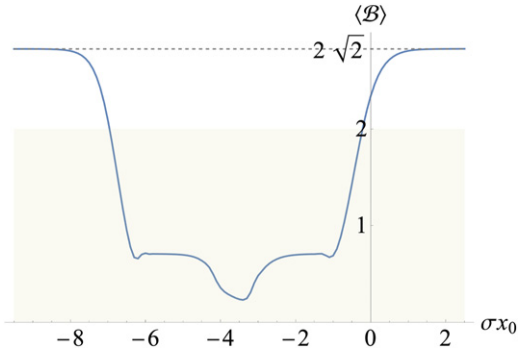

Figure 9. BIV in an Alcubierre metric as a function of the initial center point x_0 between left and right wavepackets. The shaded area corresponds to values of $\langle\hat{\mathcal{B}}\rangle$ that are compatible with classical random variables.

annihilation operators in the same way as in flat space and assume that

$$\hat{a}_{\bar{\psi}_{\pm\mathrm{R}}}|0\rangle = \hat{a}_{\bar{\psi}_{\pm\mathrm{L}}}|0\rangle = 0. \tag{60}$$

We consider the situation that the detector wavepackets are identical to the initial photon wavepackets, but that they are displaced in such a way that their peak matches that of the propagating wavepackets at the time of measurement. This is done to maximize the overlap between the two sets of wavepackets. Since the left-moving photon only travels through flat space, this implies that $\bar{\psi}_{+\mathrm{R}} = \psi_{+\mathrm{R}}$ and $\bar{\psi}_{+\mathrm{L}} = \psi_{+\mathrm{L}}$. However, since the right moving wavepackets $\psi_{-\mathrm{R}}, \psi_{-\mathrm{L}}$ are distorted by gravity, their overlap with the respective detector wavepackets $\bar{\psi}_{-\mathrm{R}}$ and $\bar{\psi}_{-\mathrm{L}}$ will generally not be unity.

Evaluating the mean value of the Bell operator $\hat{\mathcal{B}} = \sqrt{2}(\hat{\sigma}_{x+}\hat{\sigma}_{x-} + \hat{\sigma}_{z+}\hat{\sigma}_{z-})$ in state (56) amounts to a repeated application of equations (39) and (60). The result is lengthy but can be greatly simplified if one takes into account that $\langle\bar{\psi}_{+\mathrm{R}}|\psi_{+\mathrm{R}}\rangle = \langle\bar{\psi}_{+\mathrm{L}}|\psi_{+\mathrm{L}}\rangle = 1$ and $\langle\bar{\psi}_{+\mathrm{R}}|\psi_{+\mathrm{L}}\rangle = \langle\bar{\psi}_{+\mathrm{L}}|\psi_{+\mathrm{R}}\rangle = 0$. We then arrive at

$$\langle\psi|\hat{\mathcal{B}}|\psi\rangle = \frac{1}{\sqrt{2}}\left(\left|\langle\bar{\psi}_{-\mathrm{R}}|\psi_{-\mathrm{R}}\rangle + \langle\bar{\psi}_{-\mathrm{L}}|\psi_{-\mathrm{L}}\rangle\right|^2 - \left|\langle\bar{\psi}_{-\mathrm{R}}|\psi_{-\mathrm{L}}\rangle - \langle\bar{\psi}_{-\mathrm{L}}|\psi_{-\mathrm{R}}\rangle\right|^2\right). \tag{61}$$

We have evaluated expression (61) numerically with the same numerical parameters for wavepackets as in section 6, and with a displacement of $\pm 5\Delta X$ for wavepackets R and L relative to the center point x_0 between them. The result is shown in figure 9. For values $\sigma x_0 < -8$, the right-moving photon will not enter the region of curvature and the Bell inequality remains maximally violated. This is also the case for values $\sigma x_0 > 1$, when the photon is dragged along with the warp drive but does not pass through curvature. For intermediate values of x_0, deformation of the wavepackets through spacetime curvature leads to such a strong reduction of $\langle\hat{\mathcal{B}}\rangle$ that the measured correlations are in line with the upper bound 2 of the CHSH inequality (shaded area in figure 9). The overall shape of the curve results from the fact that for values $\sigma x_0 \in (-8, -5)$ only the right (R) wavepacket passes through the region of curvature, and for values $\sigma x_0 \in (-3, 0)$ only the left wavepacket passes through it. Between these two intervals, both wavepackets pass through warp-induced curvature.

8. Expansion of the field operator in terms of localized wavepackets

In section 4, we have proposed a method to define annihilation operators for localized wavepackets with positive frequency. This is sufficient to describe processes that only involve a few particles, but for many applications, an expansion of the field operator in terms of annihilation and creation operators is required. In this section we will follow the ideas of reference [40] and use an over-completeness relation for wavepackets of the form (30) to derive an explicit expression for the field operator in terms of local creation and annihilation operators.

The expansion of quantum fields in terms of coherent states [41] is basically an expansion in terms of Gaussian wavepackets. In our notation, it is not hard to see that

$$\int_{-\infty}^{\infty} \mathrm{d}X_0 \int_{-\infty}^{\infty} \mathrm{d}k\, \Psi^*_{X_0,k}(T_0,Y)\Psi_{X_0,k}(T_0,X) = 2\pi^{\frac{3}{2}}\Delta X|N|^2\delta(X-Y). \tag{62}$$

Up to the hitherto unspecified normalization factor N, this is equivalent to the over-completeness relation for coherent states. Usually, coherent states are normalized according to the non-relativistic inner product for the Schrödinger equation. To adapt this to the Klein–Gordon equation in curved space, we add to the initial wavepacket (30) a second initial condition,

$$\sqrt{g_\Sigma}\nabla_n \Psi_{X_0,k}(T_0,X) = -\mathrm{i}\tilde{E}(k)\Psi_{X_0,k}(T_0,X), \tag{63}$$

with $\tilde{E}(k) \geqslant 0$. For our purpose, this factor can be chosen freely, but the choice of $\tilde{E}(k)$ determines physical properties of the wavepacket. In flat space, one would normally choose the mean energy $\tilde{E}(k) = \sqrt{k^2+m^2}$. Using inner product (36), the wavepacket is then normalized to unity for $N = 1/\sqrt{2\tilde{E}(k)\Delta X\sqrt{\pi}}$, and the overlap between two localized wavepackets is given by

$$\begin{aligned}\langle \Psi_{X_0,k}|\Psi_{X_1,k_1}\rangle = \frac{E(k)+E(k_1)}{2\sqrt{E(k)E(k_1)}}\,\exp\Bigg(&-\frac{(k-k_1)^2}{4}\Delta X^2\\ &-\frac{(X_0-X_1)^2}{4\Delta X^2}+\frac{\mathrm{i}}{2}(X_0-X_1)(k+k_1)\Bigg).\end{aligned} \tag{64}$$

A straightforward integration shows that these relativistic modes obey the over-completeness relation

$$\begin{aligned}\mathrm{i}\int_{-\infty}^{\infty}\mathrm{d}X_0\int_{-\infty}^{\infty}\mathrm{d}k\sqrt{g_\Sigma}\,\big(&\Psi^*_{X_0,k}(X,T_0)\nabla_n\Psi_{X_0,k}(Y,T_0)\\ &-(\nabla_n\Psi_{X_0,k}(X,T_0))^*\Psi_{X_0,k}(Y,T_0)\big) = 2\pi\delta(X-Y).\end{aligned} \tag{65}$$

It is shown in appendix C that this relativistic over-completeness relation leads to the following expansion of the Klein–Gordon field operator in terms of localized Gaussian wavepackets,

$$\hat{\phi}(X,T_0) = \frac{1}{2\pi}\int_{-\infty}^{\infty}\mathrm{d}X_0\int_{-\infty}^{\infty}\mathrm{d}k\left(\hat{a}_{\Psi_{X_0,k}}\Psi_{X_0,k}(X,T_0)+\hat{b}^\dagger_{\Psi^*_{X_0,k}}\Psi^*_{X_0,k}(X,T_0)\right). \tag{66}$$

Hence, it is possible to expand the field operator in terms of localized wavepackets that have an unambiguous interpretation in terms of positive and negative frequencies.

The derivation of result (66) has only made use of the properties of a conformally flat metric (21), not of the specific form of the Alcubierre metric. It therefore holds for any two-dimensional spacetime. We anticipate that similar relations can be derived for higher-dimensional spacetimes as well, as long as they have sufficiently high symmetry. It should be easy to extend equation (66) for spatially flat models, for instance. However, in absence of symmetries, it may be difficult to derive an over-completeness relation for localized wavepackets.

9. Conclusion

We have presented an exactly solvable model for 2D photon propagation near the edge of a warp drive. Explicit expressions (4), (5) for light-ray coordinates enable us to construct a family (32) of solutions for localized Gaussian wavepackets. For a given spacelike hypersurface, these solutions possess an unambiguous interpretation in terms of positive and negative mean frequencies. However, for a different choice of hypersurface, the envelope of the wavepacket and the magnitude of its mean frequency may be altered. This also happens in flat regions of spacetime, where different observers may come to different conclusions. Figure 3 shows an example, where an observer outside the warp drive would consider horizontal lines as spacelike hypersurfaces, whereas an observer inside the warp drive may consider the solid blue lines of constant T instead, even after the drive has stopped moving.

To describe quantized localized wavepackets, we have developed a method that uses the Pauli–Jordan propagator and the conserved scalar product. The method can be used in a more general setting, including a higher-dimensional spacetime, massive scalar fields, and non-Hermitian scalar fields. We have applied this theory to describe the reduction of fringe visibility in a single-photon Mach–Zehnder interferometer, and the non-violation of the CHSH inequality when wavepackets pass through a region with spacetime curvature.

Furthermore, we derived an expansion (66) of the field operator in terms of annihilation operators for localized wavepackets with positive frequency. This expansion looks similar to an expansion in terms of energy eigenstates, but it is very different in nature. First, it does not require a symmetry. Second, it is based on an over-completeness relation and does not utilize a set of basis vectors. Equation (64) demonstrates that localized wavepackets are not orthonormal, so that calculations that employ expansion (66) will generally involve integrals over mean position and wavenumber of the wavepackets.

The purpose of this work is to provide an exactly solvable example for concepts that are usually presented in a more abstract form, including local observables, horizon formation, and the observer-dependence of physical properties like mean frequency or envelope of a wavepacket. Future work may apply the expansion in terms of localized wavepackets in cosmological problems, or to study the dynamics of the energy–momentum tensor during horizon formation.

Acknowledgments

We are grateful to the Natural Sciences and Engineering Research Council of Canada (NSERC) for financial support.

Data availability statement

All data that support the findings of this study are included within the article.

Appendix A. Derivation of light ray coordinates

For the metric under consideration, equation (3) for null geodesics takes the explicit form

$$0 = (\dot{x} - \dot{z}f(x - z(t)) - 1)(\dot{x} - \dot{z}f(x - z(t)) + 1), \tag{A1}$$

which is equivalent to

$$\dot{x} = -\eta + \dot{z}f(x - z(t)), \tag{A2}$$

with $\eta = \pm 1$. To solve equation (A2), we distinguish between the cases $x > z(t)$ and $x < z(t)$. For $x < z(t)$, we make the ansatz $x(t) = -\eta t + u(t)$, which results in

$$\dot{u}\,\mathrm{e}^{-2\sigma u} = \frac{1}{2}\dot{z}\,\mathrm{e}^{-2\eta\sigma t - 2\sigma z(t)}. \tag{A3}$$

This equation can be integrated to yield

$$\mathrm{e}^{-2\sigma u(t)} - \mathrm{e}^{-2\sigma u(t_0)} = -L_\eta(t), \tag{A4}$$

where t_0 is a fixed time and L_η is given by equation (6). Ideally, t_0 is a time such that $\dot{z}(t \leqslant t_0) = 0$ because the hypersurface t_0 is then spacelike everywhere.

In the case $x > z(t)$, we make the ansatz $x(t) = -\eta t + z(t) + u(t)$, to obtain

$$\dot{u}\,\mathrm{e}^{2\sigma u} = -\frac{\dot{z}}{2}\,\mathrm{e}^{2\eta\sigma t}. \tag{A5}$$

Integrating this yields

$$\mathrm{e}^{2\sigma u} - \mathrm{e}^{2\sigma u(t_0)} = -R_\eta(t), \tag{A6}$$

with R_η given by equation (7). Re-expressing everything in terms of x, we obtain

$$\mathrm{e}^{-2\sigma(x(t)+\eta t)} - \mathrm{e}^{-2\sigma(x_0+\eta t_0)} = -L_\eta(t) \quad \text{for } x < z(t) \tag{A7}$$

$$\mathrm{e}^{2\sigma(x(t)+\eta t - z(t))} - \mathrm{e}^{2\sigma(x_0+\eta t_0 - z(t_0))} = -R_\eta(t) \quad \text{for } x > z(t). \tag{A8}$$

Solving these equations for x and denoting the result by $\mathcal{X}_\eta(t)$ provides us with the trajectory for light rays,

$$\mathcal{X}^{\mathrm{L}}_\eta(t) = -\eta t - \frac{1}{2\sigma}\,\ln\left(\mathrm{e}^{-2\sigma(x_0+\eta t_0)} - L_\eta(t)\right) \tag{A9}$$

$$\mathcal{X}^{\mathrm{R}}_\eta(t) = -\eta t + z(t) + \frac{1}{2\sigma}\,\ln\left(\mathrm{e}^{2\sigma(x_0+\eta t_0 - z(t_0))} - R_\eta(t)\right). \tag{A10}$$

Here, $\mathcal{X}^{\mathrm{L}}_\eta(t)$ is valid for the region $x < z(t)$, and $\mathcal{X}^{\mathrm{R}}_\eta(t)$ is valid for the region $x > z(t)$.

To find light ray coordinates $x_\pm$, we employ the method of characteristic lines. This amounts to solving the equation $\mathcal{X}_\eta(t) = x$ for a constant of motion, which then corresponds

to light ray coordinates $\bar{x}_\eta$. We chose this constant to be $\bar{x}_\eta = x_0 + \eta t_0$, which results in equations (4) and (5).

Appendix B. Proof of equation (39)

We begin by recapitulating some properties of the Pauli–Jordan propagator. Its general form in $n+1$ dimensional Minkowski space is given by

$$G_{\mathrm{PJ}}^{\mathrm{Mink}}(x,y) = \frac{1}{(2\pi)^n}\int \frac{\mathrm{d}^n k}{E(k)}\,\sin(k_\mu(x^\mu - y^\mu)), \tag{B1}$$

with $\mathbf{k}$ an n-dimensional spatial vector and $k_\mu = (-E(k), \mathbf{k})$. We work with the general energy–momentum dispersion relation $E(k) = \sqrt{k^2 + m^2}$, which reduces to $E(k) = |\mathbf{k}|$ for photons. Explicit expressions for the Pauli–Jordan function for massless particles in 4D and 2D are given by [9, 42]

$$G_{\mathrm{PJ}}^{(4\mathrm{D}),\mathrm{Mink}}(x,y) = \frac{\theta(y^0 - x^0) - \theta(x^0 - y^0)}{2\pi}\delta\left((x-y)_\mu(x-y)^\mu\right) \tag{B2}$$

$$G_{\mathrm{PJ}}^{(2\mathrm{D}),\mathrm{Mink}}(x,y) = -\frac{1}{2}\theta\left(-(x-y)_\mu(x-y)^\mu\right). \tag{B3}$$

We remark that the authors of reference [9] introduce a frequency cutoff to remove a logarithmic long-wavelength divergence that appears in two spacetime dimensions. However, since we consider wavepackets of finite width, infrared renormalization is not required [42].

By definition, the Pauli–Jordan function is antisymmetric under exchange of coordinates. The support of G_{PJ} lies within the light cone, $-\Delta x_\mu \Delta x^\mu \geqslant 0$. For the proof of equation (39), we will need the following additional properties. Let n^μ be a future-oriented unit vector and $\Lambda^{\mu'}_{\ \nu}$ a Lorentz transformation such that $n^{\mu'} = (1,0,0,\ldots)$ is parallel to the new time axis. In this frame, $x^{\mu'} = (x^{0\prime}, \mathbf{x}')$. Furthermore, set $\nabla_{n,x} = n^\mu \frac{\partial}{\partial x^\mu}$. Then

$$\lim_{y^{0\prime}\to x^{0\prime}} G_{\mathrm{PJ}}(x,y) = 0 \tag{B4}$$

$$\lim_{y^{0\prime}\to x^{0\prime}} \nabla_{n,x} G_{\mathrm{PJ}}(x,y) = -\delta_\Sigma(x-y) \tag{B5}$$

$$\lim_{y^{0\prime}\to x^{0\prime}} \nabla_{n,x}\nabla_{n,y} G_{\mathrm{PJ}}(x,y) = 0. \tag{B6}$$

Here, we have introduced the notation

$$\delta_\Sigma(x-y) = \delta(\mathbf{x}' - \mathbf{y}') \tag{B7}$$

for the Dirac distribution on a spatial hypersurface Σ with normal vector n^μ. For a point $x \in \Sigma$, it fulfills

$$\int_\Sigma \mathrm{d}\Sigma \sqrt{g_\Sigma(y)}\,\delta_\Sigma(x-y) f(y) = f(x). \tag{B8}$$

The proof of these relations uses equation (B1) and the fact that measure $\mathrm{d}^n k/E(\mathbf{k})$ is Lorentz invariant. Equations (B4) and (B6) then follow from the antisymmetry of the integrands, and equation (B5) from a direct calculation.

In a curved spacetime, the Pauli–Jordan function is still antisymmetric and also obeys equations (B4)–(B6). To understand this, consider a point $x \in \Sigma$ on a spacelike hypersurface

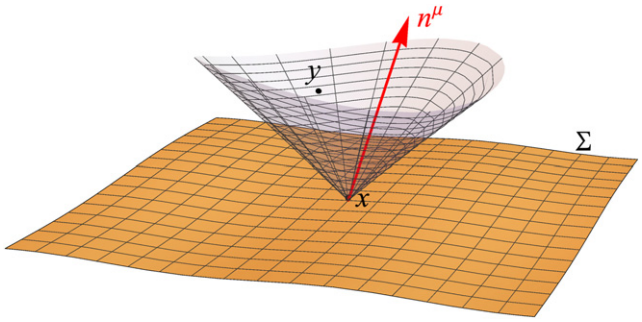

Figure 10. Sketch of the support of the Pauli–Jordan function for a point x on a spatial hypersurface Σ, a second point y, and a future-directed unit vector n^μ.

with normal vector $n^\mu(x)$. In the limit that y approaches Σ, the support of $G_{\rm PJ}(x,y)$ shrinks to a single point on the hypersurface, see figure 10. Since spacetime is locally flat, we can use Riemann normal coordinates to express $G_{\rm PJ}$ in a (infinitesimally small) neighborhood around point x. In these coordinates, the Pauli–Jordan function will take the same form as in flat space and therefore will also obey equations (B4)–(B6).

Let Σ' be a second hypersurface that is displaced from Σ by a small amount in the direction of n^μ. That means, for every point $x\in\Sigma$, we can find another point $y\in\Sigma'$ such that $y^\mu = x^\mu + \epsilon\Delta x(x) n^\mu$ for some bounded function $\Delta x(x)$ and a small parameter ϵ. The limit $\Sigma'\to\Sigma$ then corresponds to the uniform limit $\epsilon\to 0$. We can use this to evaluate commutator (39) as follows,

$$
\begin{aligned}
[\hat a_\psi(\Sigma),\hat a_\chi^\dagger(\Sigma)] = \lim_{\Sigma'\to\Sigma}\Bigg[&\mathrm{i}\int \mathrm{d}\Sigma\sqrt{g_\Sigma(x)}\left(\psi^*(x)\nabla_{n,x}\hat\phi(x) - (\nabla_{n,x}\psi^*(x))\hat\phi(x)\right),\\
&-\mathrm{i}\int \mathrm{d}\Sigma'\sqrt{g_{\Sigma'}(y)}\left(\chi(y)\nabla_{n,y}\hat\phi^\dagger(y) - (\nabla_{n,y}\chi(y))\hat\phi^\dagger(y)\right)\Bigg] \qquad \text{(B9)}\\
= \lim_{\Sigma'\to\Sigma}\int \mathrm{d}\Sigma\sqrt{g_\Sigma(x)}\int \mathrm{d}\Sigma'\sqrt{g_{\Sigma'}(y)}\Big\{&\psi^*(x)\chi(y)\nabla_{n,y}\nabla_{n,x}\mathrm{i}G_{\rm PJ}(x,y)\\
&-(\nabla_{n,x}\psi^*(x))\chi(y)\nabla_{n,y}\mathrm{i}G_{\rm PJ}(x,y) - \psi^*(x)(\nabla_{n,y}\chi(y))\nabla_{n,x}\mathrm{i}G_{\rm PJ}(x,y)\\
&+(\nabla_{n,x}\psi^*(x))(\nabla_{n,y}\chi(y))\mathrm{i}G_{\rm PJ}(x,y)\Big\} \qquad \text{(B10)}\\
= \mathrm{i}\int \mathrm{d}\Sigma\sqrt{g_\Sigma(x)}\int \mathrm{d}\Sigma\sqrt{g_\Sigma(y)}\Big\{&-(\nabla_{n,x}\psi^*(x))\chi(y)\delta_\Sigma(x-y)\\
&+\psi^*(x)(\nabla_{n,y}\chi(y))\delta_\Sigma(x-y)\Big\} \qquad \text{(B11)}\\
= \langle\psi|\chi\rangle. \qquad &\text{(B12)}
\end{aligned}
$$

For completeness, we also mention that for a conformally flat metric (21), the retarded Green's function for massless particles in curved space is related to the Green's function in Minkowski space via

$$
G_{\rm ret}(x,y) = \sqrt{g_\Sigma(y)}\,G^{\rm Mink}_{\rm ret}(x,y). \qquad \text{(B13)}
$$

It is therefore easy to find an explicit expression for the Pauli–Jordan propagator for the case studied in this paper.

Appendix C. Proof of equation (66)

Inserting definitions (37), (38) of mode operators, we find

$$\frac{1}{2\pi}\int_{-\infty}^{\infty}\mathrm{d}X_0\int_{-\infty}^{\infty}\mathrm{d}k\left(\hat{a}_{\Psi_{X_0,k}}\Psi_{X_0,k}(X,T_0)+\hat{b}^{\dagger}_{\Psi^*_{X_0,k}}\Psi^*_{X_0,k}(X,T_0)\right) \tag{C1}$$

$$\begin{aligned}=\frac{1}{2\pi}\int_{-\infty}^{\infty}\mathrm{d}X_0\int_{-\infty}^{\infty}\mathrm{d}k\int\mathrm{d}Y\sqrt{g_\Sigma}\Big\{&\Psi_{X_0,k}(X,T_0)\mathrm{i}\left(\Psi^*_{X_0,k}(Y)\nabla_n\hat{\phi}(Y)\right.\\&\left.-(\nabla_n\Psi_{X_0,k}(Y))^*\hat{\phi}(Y)\right)-\mathrm{i}\Psi^*_{X_0,k}(X,T_0)\left(\Psi_{X_0,k}(Y)\nabla_n\hat{\phi}(Y)\right.\\&\left.-(\nabla_n\Psi_{X_0,k}(Y))\hat{\phi}(Y)\right)\Big\}\end{aligned} \tag{C2}$$

$$\begin{aligned}=\frac{\mathrm{i}}{2\pi}\int\mathrm{d}Y\sqrt{g_\Sigma}\int_{-\infty}^{\infty}\mathrm{d}X_0\int_{-\infty}^{\infty}\mathrm{d}k\Big\{&\nabla_n\hat{\phi}(Y)\left(\Psi_{X_0,k}(X,T_0)\Psi^*_{X_0,k}(Y)\right.\\&\left.-\Psi^*_{X_0,k}(X,T_0)\Psi_{X_0,k}(Y)\right)+\hat{\phi}(Y)\left(\Psi^*_{X_0,k}(X,T_0)(\nabla_n\Psi_{X_0,k}(Y))\right.\\&\left.-\Psi_{X_0,k}(X,T_0)(\nabla_n\Psi_{X_0,k}(Y))^*\right)\Big\}.\end{aligned} \tag{C3}$$

It is not hard to see that the term multiplying $\nabla_n\hat{\phi}(Y)$ in the last expression is antisymmetric in k. Consequently, the integral over k for this term will be zero and we are left with

$$\begin{aligned}&\frac{1}{2\pi}\int_{-\infty}^{\infty}\mathrm{d}X_0\int_{-\infty}^{\infty}\mathrm{d}k\left(\hat{a}_{\Psi_{X_0,k}}\Psi_{X_0,k}(X,T_0)+\hat{b}^{\dagger}_{\Psi^*_{X_0,k}}\Psi^*_{X_0,k}(X,T_0)\right)\\&\quad=\frac{1}{2\pi}\int\mathrm{d}Y\hat{\phi}(Y)\times\int_{-\infty}^{\infty}\mathrm{d}X_0\int_{-\infty}^{\infty}\mathrm{d}k\mathrm{i}\sqrt{g_\Sigma}\left(\Psi^*_{X_0,k}(X,T_0)\right.\\&\qquad\left.\times(\nabla_n\Psi_{X_0,k}(Y))-\Psi_{X_0,k}(X,T_0)(\nabla_n\Psi_{X_0,k}(Y))^*\right)\end{aligned} \tag{C4}$$

$$=\frac{1}{2\pi}\int\mathrm{d}Y\hat{\phi}(Y)2\pi\delta(X-Y) \tag{C5}$$

$$=\hat{\phi}(X,T_0). \tag{C6}$$

ORCID iDs

Karl-Peter Marzlin https://orcid.org/0000-0001-8800-1697

References

[1] Fulling S A 1989 *Aspects of Quantum Field Theory in Curved Space-Time* (Cambridge: Cambridge University Press)

[2] Alcubierre M 1994 *Class. Quantum Grav.* **11** L73
[3] Anninos P, Bernstein D, Brandt S R, Hobill D, Seidel E and Smarr L 1994 *Phys. Rev.* D **50** 3801
[4] Alcubierre M, Brandt S, Brügmann B, Gundlach C, Massó J, Seidel E and Walker P 2000 *Class. Quantum Grav.* **17** 2159
[5] Dimock J 1980 *Commun. Math. Phys.* **77** 219
[6] Hollands S and Wald R M 2015 *Phys. Rep.* **574** 1
[7] Wald R 2009 *Proc. of the beyond Einstein Conf.*
[8] Sorkin R D 2011 *J. Phys.: Conf. Ser.* **306** 012017
[9] Afshordi N, Buck M, Dowker F, Rideout D, Sorkin R D and Yazdi Y K 2012 *J. High Energy Phys.* JHEP10(2012)88
[10] Brunetti R, Fredenhagen K and Verch R 2003 *Commun. Math. Phys.* **237** 31
[11] Brunetti R and Fredenhagen K 2009 Quantum field theory on curved backgrounds *Quantum Field Theory on Curved Spacetimes* (*Lecture Notes in Physics*) (Berlin: Springer) pp 129–55
[12] Fredenhagen K and Rejzner K 2016 *J. Math. Phys.* **57** 031101
[13] Bär C and Ginoux N 2012 *Global Differential Geometry* ed C Bär, J Lohkamp and M Schwarz (Berlin: Springer) pp 359–400
[14] Bär C 2015 *Commun. Math. Phys.* **333** 1585
[15] Clauser J F, Horne M A, Shimony A and Holt R A 1969 *Phys. Rev. Lett.* **23** 880
[16] Clark C, Hiscock W A and Larson S L 1999 *Class. Quantum Grav.* **16** 3965
[17] Anderson T H, Mackay T G and Lakhtakia A 2011 *J. Opt.* **13** 055107
[18] Müller T and Weiskopf D 2012 *Gen. Relativ. Gravit.* **44** 509
[19] Smolyaninov I I 2011 *Phys. Rev.* B **84** 113103
[20] Hiscock W A 1997 *Class. Quantum Grav.* **14** L183
[21] Smyth R 1996 *Proc. Am. Math. Soc.* **124** 1559
[22] Lichnerowicz A 1961 *Publ. Math. Inst. Hautes Sci.* **10** 5
[23] Birrell N D and Davies P C W 1984 *Quantum Fields in Curved Space* (Cambridge: Cambridge University Press)
[24] Parker L and Toms D 2009 *Quantum Field Theory in Curved Spacetime* (Cambridge: Cambridge University Press)
[25] Jacobson T 2003 *Lectures Given at the CECS School on Quantum Gravity* (Valdivia, Chile January 2002)
[26] Wald R M 2006 The history and present status of quantum field theory in curved spacetime *Einstein and the Changing Worldviews of Physics* ed C Lehner, J Renn and M Schemmel (Boston, MA: Birkhäuser) pp 317–31
[27] Barbado L, Barceló C, Garay L and Jannes G 2016 *Phys. Rev.* D **94** 064004
[28] Junker W and Schrohe E 2002 *Ann. Henri Poincare* **3** 1113
[29] Dolby C 2006 Simultaneity and the concept of 'particle' *Time and Matter* ed I Bigi and M Faessler (Singapore: World Scientific) pp 145–57
[30] Walls D and Milburn G J 2008 *Quantum Optics* (Berlin: Springer)
[31] Bell J S 1964 *Physics* **1** 195
[32] Aspect A, Dalibard J and Roger G 1982 *Phys. Rev. Lett.* **49** 1804
[33] Tsirel'son B S 1987 *J. Sov. Math.* **36** 557
[34] Banaszek K and Wódkiewicz K 1998 *Phys. Rev.* A **58** 4345
[35] Banaszek K and Wódkiewicz K 1999 *Phys. Rev. Lett.* **82** 2009
[36] Chen Z-B, Pan J-W, Hou G and Zhang Y-D 2002 *Phys. Rev. Lett.* **88** 040406
[37] Gour G, Khanna F C, Mann A and Revzen M 2004 *Phys. Lett.* A **324** 415
[38] Praxmeyer L, Englert B-G and Wódkiewicz K 2005 *Eur. Phys. J.* D **32** 227
[39] Marcikic I, de Riedmatten H, Tittel W, Zbinden H, Legré M and Gisin N 2004 *Phys. Rev. Lett.* **93** 180502
[40] Palmer M C, Takahashi M and Westman H F 2012 *Ann. Phys., NY* **327** 1078
[41] Cahill K E and Glauber R J 1969 *Phys. Rev.* **177** 1857
[42] Scharf G 2014 *Finite Quantum Electrodynamics* 3rd edn (New York: Dover)